Can we gain knowledge on COS anthropogenic and biogenic emissions from a single atmospheric mixing ratios measurement site?

Antoine Berchet[1], Isabelle Pison[1], Camille Huselstein[1], Clément Narbaud[1], Marine Remaud[1,2], Sauveur Belviso[1], Camille Abadie[1], and Fabienne Maignan[1]

[1]Laboratoire des Sciences du Climat et de l'Environnement, CEA-CNRS-UVSQ, Gif-sur-Yvette, France
[2]now at: Faculty of Science, A-LIFE, Vrije Universiteit Amsterdam, 1081 HV Amsterdam, the Netherlands

Correspondence to: antoine.berchet@lsce.ipsl.fr, isabelle.pison@lsce.ipsl.fr

Abstract. Lack of knowledge still remains on many processes leading to COS atmospheric fluxes, either natural such as the oceanic emissions or the vegetation and soil fluxes, or anthropogenic, from industrial activities and power generation. Moreover, COS atmospheric mixing ratio data are still too sparse to evaluate the estimations of these sources and sinks. This study assesses the anthropogenic and biogenic COS fluxes at the regional scale, in the footprint a measurement site in Western

5 Europe, at a seasonal to diurnal time resolution over half a decade. The continuous time series of COS mixing ratios obtained at the monitoring site of Gif-sur-Yvette (in the Paris area) from August 2014 to December 2019 are compared to simulations with the Lagrangian model FLEXPART, transporting oceanic emissions, biogenic land fluxes from the process-model ORCHIDEE and anthropogenic emissions by two different inventories. The anthropogenic emission inventory based on reported industrial emissions and the characteristics of coal power plants in Europe is consistent with the observations. The flat temporal variability

10 applied to anthropogenic fluxes due to lack of information on industrial and power-generation activity in viscose factories and coal-power plants and the potential mismatches in the representation of the plumes emitted from these hot-spots in the model are the main limitations of this inventory. We find that the net ecosystem COS uptake simulated by ORCHIDEE is underestimated in winter at night, which suggests improvements in the parameterization of the nighttime uptake by plants for COS.

1 Introduction

15 Carbonyl sulfide (COS) is absorbed along CO_2 by plants during photosynthesis. But COS, contrary to CO_2, is almost not emitted during respiration-like processes (Protoschill-Krebs et al., 1996; Montzka et al., 2007; Sandoval-Soto et al., 2005). This has led to thinking that COS could be used as a tracer for quantifying and/or reducing uncertainties on CO_2 fluxes due to photosynthesis (Whelan et al., 2018, and references within).

  The methodology called atmospheric inversion consists in assimilating mixing ratio data into a statistical framework (called

20 Bayesian because it is based on Bayes'theorem) making use of some prior knowledge of sources and sinks and of a chemistry-transport model (CTM) to link fluxes (either emissions to the atmosphere or uptake) to atmospheric mixing ratios, in order to retrieve optimized fluxes. The optimized fluxes are statistically consistent with all the information provided in the prior

knowledge of sources and sinks and in the measured atmospheric mixing ratios. The minimum requirements for atmospheric inversion to yield useful insights are therefore *i)* that the CTM resolution, various inputs (such as meteorological fields, flux maps) and physical and chemical parameterizations are relevant to the targeted spatio-temporal scale, so that the link between fluxes and atmospheric mixing ratios does not entail large or poorly characterized uncertainties, but also *ii)* that the uncertainties

5 on the prior knowledge of sources and sinks are well characterized, so that the corrections applied to obtain optimized fluxes are physically meaningful. On top of these general requirements, when using COS mixing ratio data to get information on CO_2 uptake during photosynthesis, the atmospheric inversion must be provided with information that make it possible to disentangle the influence of the biogenic sink of COS from the influence of anthropogenic and other biogenic fluxes on the measured COS mixing ratios. This can be done by providing to the CTM fluxes of COS which are well-known, i.e., with small

10 and well-characterized uncertainties. It is therefore a strong limitation to today's potential use of COS to gain insight into CO_2 photosynthesis fluxes that COS sources and sinks are not very well known so far, with only a few estimations available for the various categories (Whelan et al., 2018; Remaud et al., 2023) , which can be summarized as:

- the natural oceanic source, due to both direct COS emissions and indirect emissions via dimethyl sulfide (DMS) and carbon disulfide (CS_2) (Mihalopoulos et al., 1992). Note that fresh waters also contribute to COS emissions (Du et al.,

15 2017). In the atmosphere, CS_2 is oxidized into COS in about 10 days (Bandy et al., 1981; Khalil and Rasmussen, 1984; Chin and Davis, 1993; Stickel et al., 1993). The total of direct and indirect oceanic emissions are estimated at 265 ± 210 GgS.yr^{-1} by Lennartz et al. (2017) (cited in Whelan et al., 2018) and Lennartz et al. (2021).

- anthropogenic sources of COS, restricted to particular industries, once again in contrast to CO_2. These anthropogenic sources are due to industries which emit either COS or CS_2. The main source of anthropogenic COS is the oxidation of

20 CS_2 emitted by the viscose industry which includes factories producing viscose as their final product (named hereafter viscose-producing industry) or as the by-product of their main process for producing, e.g., sponges, cellophane (Chen, 2015; Water, 2011) (named hereafter viscose processors). Other sources are smaller and emit both COS and CS_2: they are in the sector of energy production with coal use in power plants but also the combustion of oil and bio-fuels (Attar, 1978), the pulp mills due to the kraft process (Brownlee et al., 1995; Cheremisinoff and Rosenfeld, 2010), industries

25 using aluminum oxide electrolysis to produce aluminum (Harnisch et al., 1995), the producers of pigments with carbon black used for tires or the food industry and the widely used white titanium dioxide. For the whole world in the year 2012, the inventory by Zumkehr et al. (2018) gives a total of 400 ± 180 GgS.y^{-1} for all anthropogenic emissions (used in the budget elaborated by Whelan et al., 2018).

- besides the anthropogenic combustion of bio-fuels, biomass burning in open fires either natural (e.g., wild fires due to

30 lightning) or human-caused (e.g., agricultural practices) is also a source of COS, estimated at an average 60 ± 37 GgS.y^{-1} by Stinecipher et al. (2019).

- soils can also be sources of COS under specific conditions such as high temperature and incoming radiation, related to abiotic production processes (Whelan and Rhew, 2015; Whelan et al., 2016, 2018; Kitz et al., 2017, 2020). The anoxic

soil contribution has recently been estimated at 96 GgS.yr^{-1} with the ORCHIDEE process-model (Abadie et al., 2022, see also details on ORCHIDEE in Sect. 2.2.2).

– the main biogenic sink is due to the uptake of COS by vegetation (Whelan et al., 2018): COS is irreversibly consumed by the carbonic anhydrase enzyme in leaves (DiMario et al., 2016). Soils can also absorb COS due to soil microorganisms

5   that also contain the carbonic anhydrase enzyme (Masaki et al., 2021). The order of magnitude obtained for the uptake by vegetation is -530 GgS/y with the ORCHIDEE process-model (see details on ORCHIDEE in Sect. 2.2.2), to compare, for example, to -664 GgS/y with the Simple Biosphere Model (SiB4 Kooijmans et al., 2021). The oxic soils can both produce and consume COS but they are a net sink, estimated recently at -126 GgS/y with the ORCHIDEE process-model (Abadie et al., 2022). The net soil sink (taking into account the source due to anoxic soils and the net sink due to oxic

10   soils) of COS is therefore estimated at -30 GgS/yr by Abadie et al. (2022), to compare to, e.g., -89 GgS/y according to SiB4 Kooijmans et al. (2021).

– the atmospheric sink of COS is due to its oxidation by OH radicals and its photolysis in the stratosphere (estimated respectively at -130 to -80 GgS/y and -50±15 GgS/y by Whelan et al., 2018).

Reducing the uncertainties on the estimates of all these sources and sinks at the global scale at as fine temporal and spatial

15 resolutions as would be required to bring information on CO_2 fluxes due to photosynthesis does not seem easy to accomplish in the next few years. The first challenge is the lack of knowledge still remaining on many processes which lead to COS or CS_2 emissions in the atmosphere. For example, Remaud et al. (2023) conclude that a source may be missing in the Tropics (probably from the ocean) and that the uptake of COS by vegetation at high northern latitudes is too small. Some natural processes emitting COS in the atmosphere are still only suspected, for example in plants used in agriculture (Belviso et al.,

20 2022a; Maseyk et al., 2014; Bloem et al., 2012). The second difficulty is the lack of data on COS atmospheric mixing ratios, which could be used in CTMs to evaluate the available estimations of sources and sinks at the regional scale, although the National Oceanic and Atmospheric Administration (NOAA) provides atmospheric mixing ratios of COS at several stations, which are useful at the global scale. Still, NOAA data are based on monthly or at best biweekly flask samples, limiting our ability to use them to constrain fluxes at scales smaller than the global to continental scales. Observations with higher frequency

25 are very sparse globally (Belviso et al., 2020; Kamezaki et al., 2023; Zanchetta et al., 2023; Kooijmans et al., 2016; Commane et al., 2015) and were not yet used for long-term systematic assessment of regional COS fluxes.

To begin to tackle the issue, Belviso et al. (2020) have made use of one of the few continuous time series of COS atmospheric mixing ratios, available in the Paris area, to assess the budget of COS in this area at the seasonal scale and during pollution peaks. Even though the area is almost always a COS sink, local biogenic emission episodes appear in summer and

30 anthropogenic emissions from the Benelux, Eastern France and Germany are occasionally transported so as to influence the area in winter. Belviso et al. (2022b) then tried to use the information brought by the same COS time series of mixing ratios to learn more about the anthropogenic emissions in the footprint of the station, which covers part of Western Europe (including Benelux, Eastern France and Germany) and part of the Atlantic. The relatively long continuous time series made it possible to point to an issue in the oceanic and anthropogenic fluxes in this footprint but not, at this stage, to go further, e.g., characterize

accurately or even correct the issue. Following these results, Belviso et al. (2023) used a semi-quantitative approach to assess the gridded inventory of direct and indirect anthropogenic emissions of COS by Zumkehr et al. (2018) in France. The main conclusion of this work is that COS emissions in France are overestimated in this inventory by one order of magnitude and another way of mapping these emissions is required.

5 Therefore, the present study aims at building a set-up that makes it possible to quantitatively assess the anthropogenic and biogenic COS fluxes at the regional scale, i.e., in the footprint of one measurement site in Western Europe at a seasonal to diurnal time resolution over a period of half a decade. For this, we use the continuous time series of COS mixing ratios measured in the Paris area from summer 2014 to the end of year 2019, as described in Sect. 2.1. We compare them to the concentrations simulated from marine, biogenic and anthropogenic fluxes in the area of interest (detailed in Sect. 2.2) combined

10 to the contribution due to the rest of the world (Sect. 2.1) by the modeling tool described in Sect. 2.3. After an assessment of the general performances of the model (Sect. 3.1), we are able to evaluate the anthropogenic sources as estimated by Zumkehr et al. (2018) (hereafter referred to as "Zumkehr's inventory") and by our more targeted inventory (Sect. 2.2.3) and the biogenic fluxes as simulated by the ORCHIDEE processed-based land surface model (Sect. 3.3).

2 Data and methods

15 2.1 Measurements and set-up of background mixing ratios

The measurements used in this study constitute a quasi-continuous time series of COS atmospheric mixing ratios obtained at the monitoring site of Gif-sur-Yvette (GIF) located in the Paris area at 48.7109°N and 2.1476°E at 163 m asl with an inlet height 7 m agl. Gas chromatography is used to measure COS mixing ratios, as described by Belviso et al. (2016) and Belviso et al. (2020). The GIF time series of hourly data spanning from August 2014 to December 2021 is available in Belviso et al.

20 (2022b). In this study, we make use of the time series from August 2014 to December 2019 only (Fig. 1, and Fig. A1 to A6), which covers the period of availability of inputs required for simulations, in particular global concentration fields used to compute the background signal (see Sect. 2.1 and Sect. 2.3).

The time series of flask measurements sampled by the National Oceanic and Atmospheric Administration (NOAA) network at Mace Head (MHD) in Ireland at 53.3°N and 9.9°W at 42 m asl (described in Montzka et al., 2007, with 1 to 5 pairs of flask

25 per month, collected mostly between 8:00 and 17:00 UTC) are also shown in Fig. 1 to illustrate the so-called "background", i.e., the overall contribution of all the sources and sinks which are not in our area of interest. In our study, which focuses on Western Europe and more particularly on the footprint of GIF, the mixing ratios at MHD are representative of the background when the air masses are advected from the West, which is a frequent meteorological configuration (Belviso et al., 2020).

The contribution of the background to the simulated mixing ratios is computed using three-dimensional fields at the global

30 scale. The COS mixing ratio fields used here are obtained from Remaud et al. (2022), at a horizontal resolution of 3.75° in longitude and 1.875° in latitude for 39 pressure levels at a three-hourly time resolution (illustration in Fig. 2). They were designed to fit the background NOAA observation sites, such as MHD.
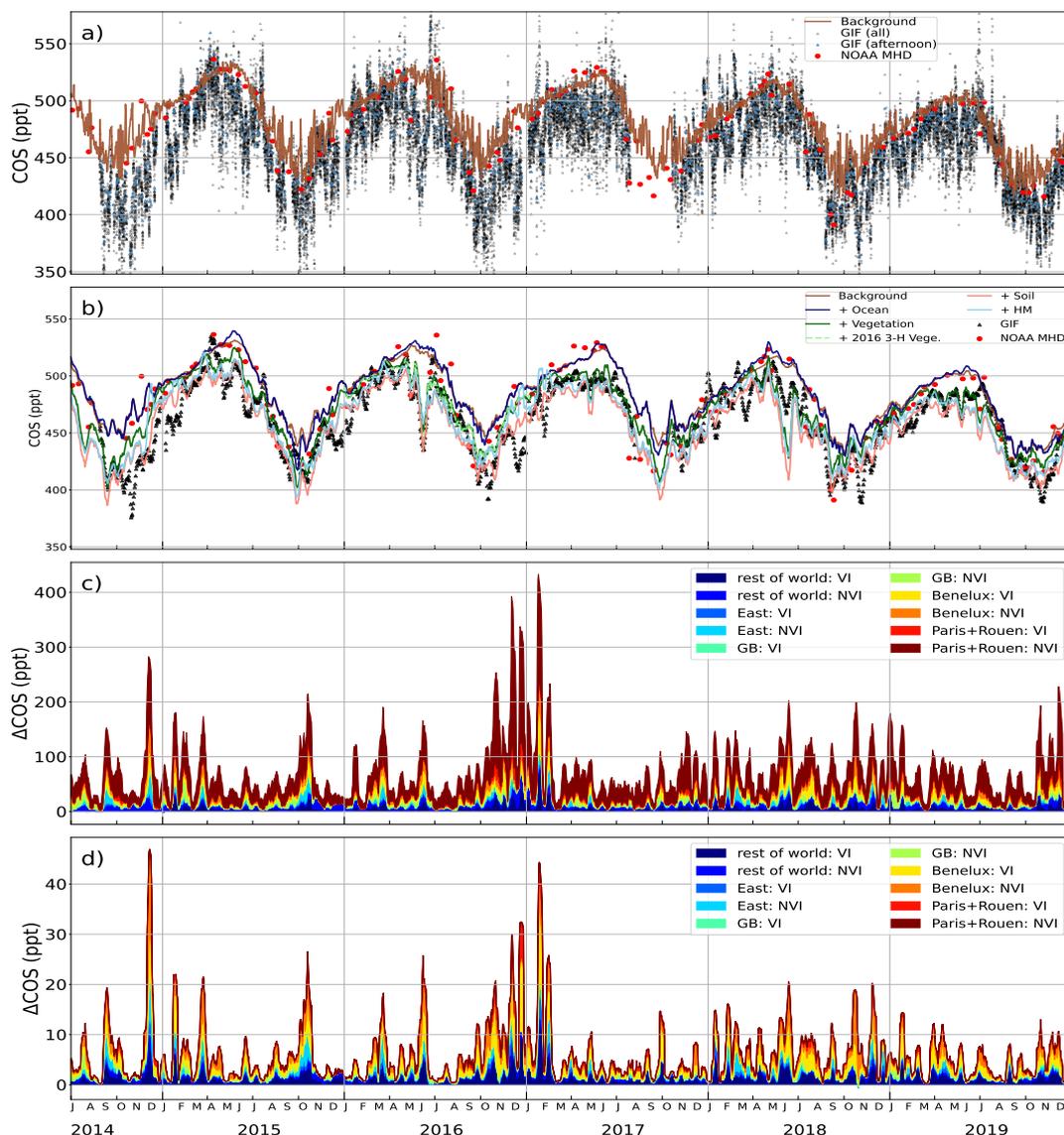
Figure 1. *Time series of observed and simulated atmospheric mixing ratios of COS. a) Hourly COS observations at GIF, with afternoon (12:00-18:00 UTC) averages super-imposed, and flask measurements at Mace Head (MHD) and simulated background described in Sect. 2.1. Remark: the limits set on the y-axis do not show $\approx$ 50 extremely low values and $\approx$ 190 extremely high values of hourly COS observations. b) 10-day rolling mean of GIF afternoon observations, with cumulative simulated contributions from background, ocean sources and biogenic land fluxes (see Sect. 2.3 for details, "2016 3-H Vege." = 3-hourly vegetation uptake as available for 2016), c) 10-day rolling mean of simulated anthropogenic contributions to COS mixing ratios by region (shown in Fig. 2) and sector according to Zumkehr's inventory (see Sect. 2.2.3, VI = viscose industry, NVI = non-viscose-related emissions), d) 10-day rolling mean of simulated contributions by region (shown in Fig. 2) and sector according to our home-made inventory ("HM", see Sect. 2.2.3, Fig. 2). Remark: afternoon data are shown here because the model is assumed to better represent the vertical mixing in the afternoon so that the comparison to measurements highlights the discrepancies in fluxes compared to the model's errors.*

2.2 Fluxes

In the following, "emission" denotes fluxes which are sources as seen from the atmosphere and "uptake" denotes fluxes which are sinks as seen from the atmosphere; "flux" is used for (ensembles of) processes which can be either sources or sinks.

Our simulations, detailed in Sect. 2.3, take into account COS fluxes in the area of interest as provided by the data sets described here. The contributions from biomass burning emissions and the atmospheric sink are neglected in this study, as well as the emissions from anoxic soils.

2.2.1 Ocean emissions

The ocean data set designed by Lennartz et al. (2021) and Lennartz et al. (2017) includes direct emissions of COS and indirect emissions of COS via CS_2 and DMS emissions at a monthly resolution and at a $1° \times 1°$ horizontal resolution. The emissions of the three species have been computed using box models calibrated with ship-borne measurements made in different parts of the globe and result in a data-driven data set for COS oceanic emissions. This ocean data set has been optimized by Remaud et al. (2022) by assimilating NOAA flask data into the model LMDZ. This optimized data-set has been compared to others by Ma et al. (2023) (therein called "OPT-LMDZ") and gives very similar results to other datasets when evaluated with independent atmospheric data. Our ocean fluxes give total (direct+indirect) emissions of COS of 507 GgS/y on average over 2014-2019 and 4 GgS/y in our domain of interest.

2.2.2 Biogenic land fluxes

In this study, biogenic land fluxes refer to vegetation uptake and soil exchanges and are simulated using the ORCHIDEE land surface model (Krinner et al., 2005). In ORCHIDEE, a mechanistic representation of vegetation COS uptake has been implemented following Berry et al. (2013), and soil COS exchanges are computed based on the model from Ogée et al. (2016), representing both COS uptake and emission by soils (see Maignan et al. (2021) and Abadie et al. (2022) for more details on the vegetation and soil models, respectively). Monthly variable near-surface COS concentrations are prescribed to compute the biogenic land fluxes. These concentrations were simulated using optimized surface COS fluxes in the LMDZ atmospheric transport model and extracted from its first vertical level (Remaud et al., 2022). Biogenic land fluxes are computed with a horizontal resolution of 1 degree × 1 degree at a monthly time-step (illustrated in Fig. 2), thus losing any temporal variability at the synoptic scale. The data set used here estimates the average uptakes of COS over 2014-2019 at 22.6 GgS/y by the vegetation and 12.9 GgS/y by the soil in our domain of interest. In particular, biogenic fluxes have a significant diurnal cycle, as COS fluxes are relative to photosynthesis occurring during day-time only. We assess the sensitivity of our simulations to daily varying biogenic fluxes by using 3-hourly vegetation uptake as simulated by ORCHIDEE for the year 2016. The difference performance of our model with monthly and 3-hourly fluxes is evaluated in Sect. 3.1.

2.2.3 Anthropogenic emissions

Two different COS anthropogenic inventories are used in this study.

Main characteristics of Zumkehr's inventory

The inventory by Zumkehr et al. (2018) accounts for the sectors emitting the most COS and CS_2 at the country level and provides yearly emissions from 1980 to 2012. Here, the values for the year 2012, as the most recent available, have been used. In our domain of interest, they amount to a total of 62.1 GgS among which 20.5 GgS for the viscose industry, 14.5 GgS for

5   coal use, 23.6 GgS for the pigments and 2.8 GgS for aluminum production. The sub-country distribution is done according to secondary proxies, such as energy industry activity or industrial CO_2 emissions. This proxy-based distribution proved efficient in the U.S., but can be misleading in some European countries. For example, in France, where coal-based energy production is almost absent and where viscose industry is limited to a handful of site, Zumkehr's methodology leads to a distribution of national emissions to many hot spots close to the main urban areas. As shown in Fig. 2 and Fig. 1c of Belviso et al. (2023),

10   such a hot spot appears in the Paris area, with its center located close (about 20 km) to the North-East of GIF.

In the following, the sectors provided in Zumkehr's inventory (Zumkehr et al., 2018, therein Tab 1) are grouped as viscose industry emissions (abbreviated as "VI"), which include the sectors named "Pulp & Paper", "Rayon Staple", "Rayon Yarn", and non-viscose-related emissions (abbreviated as "NVI"), which include the sectors named "Agricultural Chemicals", "Aluminum Smelting", "Carbon Black", "Industrial Coal", "Residential Coal", "Industrial Solvents", "Titanium Dioxide (TiO2)",

15   and "Tires". Maps and bar plots for selected European countries are available in Belviso et al. (2023) main text and supplementary material.

Home-made inventory

To overcome the caveats of Zumkehr's inventory in Western Europe, we designed our own inventory, following the conclusions of Belviso et al. (2023), and based on:

20   – explicit declaration of CS_2 emissions from the viscose industry (including rayon yarn and staple and other products such as cellulosic casings) with a comprehensive list of plants in Europe (abbreviated as "VI" and comparable to the VI emissions in Zumkehr's inventory) for the year 2018 (available at the time of the study); see details in Tab. 2-3 of Belviso et al. (2023). The total emissions in our domain of interest are ≈ 4.7 GgS/y in 2018.

– for coal, CO_2 emissions for all coal power plants in Europe (from the Global Energy Monitor's Global Coal Plant

25   Tracker) were used to estimate COS emissions for each year based on a unique emission factor (abbreviated as "NVI" and comparable to the NVI coal-related emissions in Zumkehr's inventory). We used a value of 5.7×10^{-6} molecules of COS emitted for each molecule of CO_2 during coal combustion. The average emissions over 2014-2019 are ≈ 6.5 GgS/y in our domain of interest.

Through lack of data, we did not apply any temporal profiles to viscose and coal emissions, even though they are expected

30   to strongly vary over the year, even from one week to the next one. For viscose, we applied no inter-annual variability and keep emissions stable based on the year 2018. For coal emissions, inter-annual variability is based on yearly CO_2 emission values. Compared to Zumkehr's inventory, ours (Fig. 2) displays only a few hot spots of emissions in France: 4 viscose industry sites

Fluxes from / Region	ocean	biogenic land	Zumkehr's VI	Zumkehr's NVI	home-made VI	home-made NVI
whole area of interest	o	bl				
Benelux ("B")			ZviB	ZnviB	HMviB	HMnviB
Paris+Rouen area ("U")			ZviU	ZnviU	HMviU	HMnviU
area of interest excluding Benelux and the Paris+Rouen area			ZviW	ZnviW	HMviW	HMnviW

Table 1. *FLEXPART simulations per region (shown in Fig. 2) and sector. Each cell: a group of letters indicate that the simulation is run; the same IDs are used for each violin plot in Fig. 3. "Z" = Zumkehr's inventory, "HM" = home-made inventory (this study), "VI" or "vi" = viscose industry, "NVI" or "nvi" = non-viscose-related (actually coal-related only in HM, see Sect. 2.2.3), "U" = Paris+Rouen area = an urban and industrial area, "B" = Benelux, "W" = whole area excluding "B" and "U".*

with big factories and 4 coal-burning power plants. The closer to GIF is in the city of Beauvais, which lies about 85 km to the North of GIF, i.e., further than the Paris area.

2.3 Simulations of concentrations

The modelled COS mixing ratios were obtained by using the Lagrangian atmospheric transport model FLEXPART (FLEXible
5 PARTicle) version 10.3 (Stohl et al., 2005; Pisso et al., 2019). The model FLEXPART is driven by meteorological data from the European Centre for Medium-range Weather Forecast (ECMWF) ERA5 (Hersbach et al., 2020) with 3-hourly intervals and 60 vertical layers, retrieved using the FLEX-extract toolbox (Tipka et al., 2020). In our case, meteorological data is provided to FLEXPART at a $1°$ horizontal resolution. For the whole duration of the observation period, 2000 virtual particles are released every 6 h and followed backward in time for 10 days. The multiple FLEXPART simulations are driven by the GUI-based
10 toolbox designed by Berchet et al. (2023).

We assume a conversion of CS_2 to COS with a maximum of 87% molar conversion rate, as estimated by Barnes et al. (1994) and as used by Zumkehr et al. (2018). The kinetics of the conversion is approximated by prescribing a half-life of 3 days to CS_2 in the atmosphere. The amount of COS created from a CS_2 source along the transport path of the air mass is then given as $0.87 \times \left(1 - e^{-\frac{t}{\tau \ln 2}}\right)$ with $\tau = 3$ days.
15 So called source-sensitivity (or footprint) maps (Seibert and Frank, 2004) are computed for every release date by counting the number of particles transported above a certain point below a threshold of 500 m above ground. Source contribution by process-type are inferred by convolving source-sensitivity maps with flux maps from the ocean emissions, the biogenic fluxes and one of the two anthropogenic emission inventories (see Sect. 2.2.1, Sect. 2.2.2, Sect. 2.2.3). One FLEXPART simulation is run for each process or sector and region of interest (see Fig. 2) so that the simulations (Tab. 1) can be combined to include
20 or exclude particular sectors and/or particular regions when building the footprint maps.
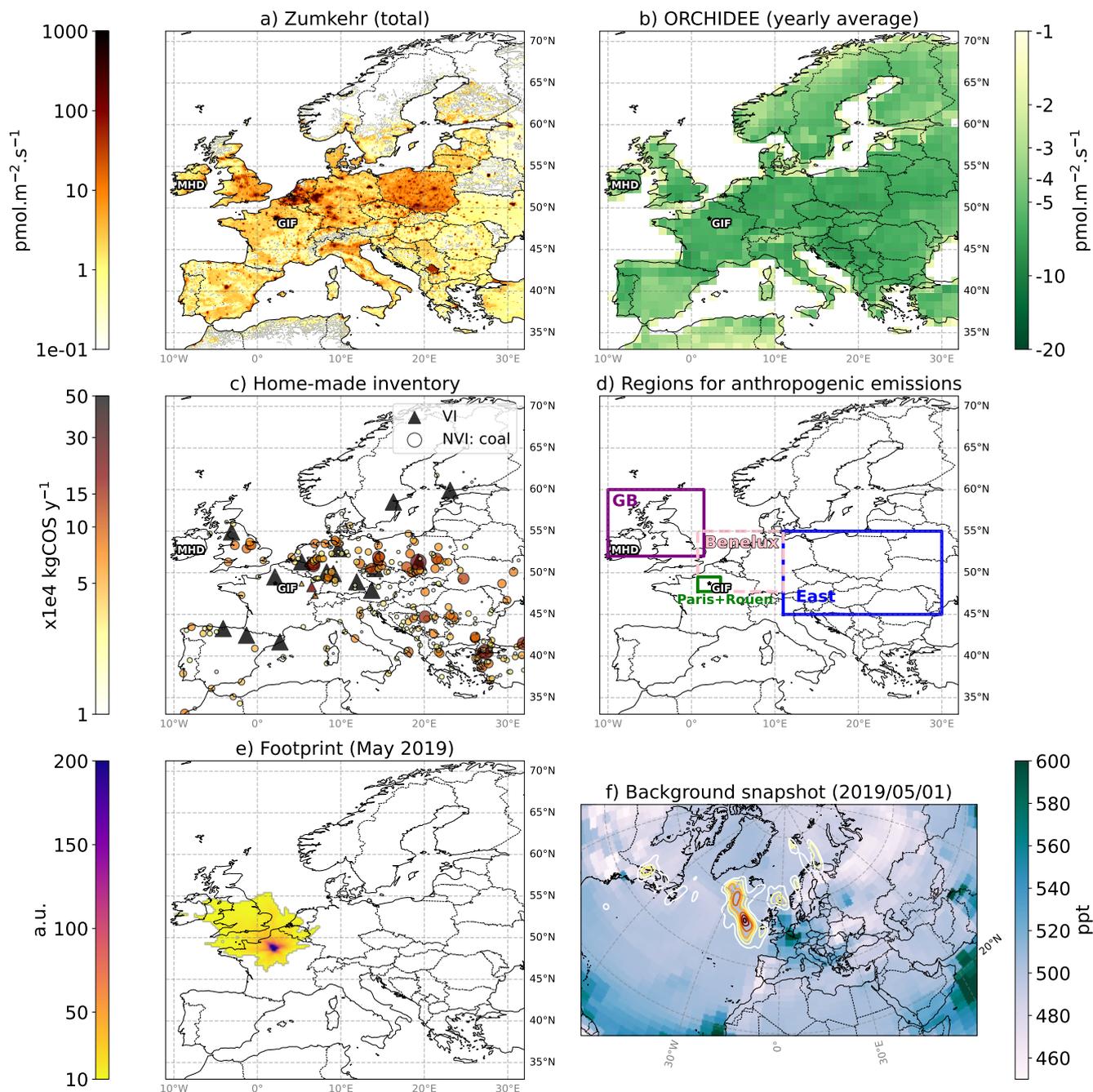
Figure 2. *Maps of input data sets used in our study. a) Zumkehr's yearly, i.e., 2012 total emissions, b) 2019 yearly average biogenic land fluxes from the ORCHIDEE model, c) emission points from viscose and coal industries as defined using our methodology (see Sect. 2.2.3 for details, here year 2019 for illustration), d) regions of interest for anthropogenic emissions, e) illustration of footprint summed-up over one month, f) snapshot of background concentration fields; contours highlight the computed sensitivity to the background 10-days before observation at GIF (see Sect. 2.3 for details). Remark: units for area (gridded) emissions are pmol.m^{-2} whereas emissions by point sources are in mass units; footprints are shown in arbitrary units (a.u.).*

The background mixing ratios (Fig. 2f) are calculated by combining the 3D source-sensitivity fields (e.g., Thompson and Stohl, 2014; Pisso et al., 2019) at the end of the backward trajectories with the available COS concentration field (see Sect. 2.1). The background thus obtained represents the average of the mixing ratios in the grid cells where each particle trajectory terminated 10 days before the observation. For instance, as illustrated in Fig. 2f, for the given date, GIF observations are sensitive

5   to background mostly in North-Western Atlantic (higher sensitivity for deep red contours). The computation of COS contributions from surface fluxes and the background was carried out using the Community Inversion Framework (CIF; Berchet et al., 2021).

3   Results and discussion

3.1   General performances of the model at GIF

10   By design, the background contribution (Sect. 2.1) fits the main monthly variations as measured at a background station such as MHD (Fig. 1 a) and b)). Its contribution at GIF ensures a good simulation of the variability (Tab. 2: Pearson's correlation ≥ 0.75) and a small mean error (RMS ≤ 35 ppt) over the whole period of interest. As expected, adding the natural emissions from the ocean (Sect. 2.2.1) and the biogenic land fluxes (Sect. 2.2.2) reduces the bias (by almost 15 ppt in absolute value) and the mean error is decreased by more than 20%.

15   As mentioned in Sect. 2.2.2, we assess the impact of using temporally resolved biogenic fluxes on our simulations. Making use of a vegetation uptake with a 3-hourly time resolution (during only the year 2016, see Sect. 2.2.2) does not improve the statistical fit of the model to the observations: the bias and RMS are almost unchanged and the correlation is decreased (Tab. 2: from 0.74 to 0.72). The variability is not better reproduced when adding the natural emissions to the background (correlation from 0.76 to 0.74, excluding the case of the 2016 3-hourly varying vegetation uptake), which may be due to too

20   coarse a variability for the ocean emissions (with a monthly resolution, Sect. 2.2.1) and an issue with the variability of the vegetation uptake or the soil exchanges, probably at the seasonal scale, which is assessed in Sect. 3.3. The limited impact, and even degradation, of performances when using the diurnal cycle of biogenic flux suggests an issue in their representation in ORCHIDEE, maybe in the residual ecosystem (vegetation and soil) COS flux simulated at night.

The contributions of the anthropogenic emissions by Zumkehr degrades all three indicators of the fit to the measured concen-

25   trations at GIF: the bias and mean error are very high (both $\geq$100 ppt), the variability is not reproduced anymore. The regional anthropogenic emissions located in the Paris+Rouen area explain the major part of the discrepancies between the simulation and the measurements (Tab. 2). According to Zumkehr's inventory, COS emissions in Île-de-France, i.e., the Paris area itself, are mostly ($\approx$62%) due to viscose industry, which is not consistent with the lack of any such factory declaring emissions in this region. The small (<1%) contribution by coal-using industry is not consistent with the last coal power-plant in the area being

30   closed in 2012. Maybe due to the same type of incomplete information or lack of relevant proxy, the overall European COS emissions in Zumkehr's inventory may be overestimated, as suggested by the very high contributions (more than 100 ppt) due to anthropogenic emissions alone simulated at GIF (Fig. 1c).

Contribution	bias (ppt)	RMS (ppt)	corr
Background	23	33	0.76
Background + ocean	23	33	0.75
Background + biogenic land	-5	25	0.73
Background + biogenic land with 2016 3-hourly vegetation	-5	26	0.71
Background + ocean + biogenic land	-5	25	0.74
Background + ocean + biogenic land with 2016 3-hourly vegetation	-4	26	0.72
Background + anthro. Zumkehr	100	151	0.11
Background + anthro. Zumkehr w/o Paris/Rouen	58	87	0.27
Background + coal (HM)	26	35	0.73
Background + viscose (HM)	25	34	0.74
Background + coal (HM) + viscose (HM)	27	37	0.71
Background + ocean + biogenic land + anthro. Zumkehr	72	129	0.14
Background + ocean + biogenic land + anthro. Zumkehr w/o Paris/Rouen	29	66	0.33
Background + ocean + biogenic land + coal HM + viscose HM	-1	25	0.74

Table 2. *Statistical indicators of the performances of the model compared to the daily afternoon (12:00-18:00 UTC) means of measurements at GIF for each contribution; indicators are computed over the whole period when measurements are available, i.e., Aug. 2014 - Dec. 2021. Bias = mean difference model minus measurement; RMS = root mean square model minus measurements; corr = Pearson's correlation coefficient between model and measurement time series. HM indicates emissions from our home-made inventory (see Sect. 2.2.3).*

The contribution of the anthropogenic emissions from our home-made inventory increases the bias and mean error compared to the contributions of the background and natural fluxes only (Tab. 2). The maximum simulated contributions are between 40 and 50 ppt for some months (Fig. 1 c and d), i.e., 10 times smaller than with Zumkehr's inventory. Therefore, the bias and mean error computed over the whole period using our inventory remain more than twice smaller than with Zumkehr without 5 the emissions of the Paris+Rouen area. This order of magnitude is more consistent with the expected anthropogenic contribution required to match the measured concentrations above the background at GIF.

The information which can be retrieved from the time series of concentrations in one measurement site on the relevancy of our inventory compared to Zumkehr's is discussed in the following in terms of activity sectors and source regions.

3.2 Anthropogenic emissions

10 The general performances of the model at GIF (Sect. 3.1) show that the total emissions of Zumkehr's inventory lead to a large overestimation of COS concentrations at GIF (Tab. 2), almost half of which is due to the emissions located in the areas of Paris and Rouen. We represent in Fig. 3 the distributions of observations and simulations from different sectors as violin plots. Above the overestimation due to the "natural" contributions, Zumkehr's inventory leads to a median overestimation of ≈52 ppt (Fig. 3, "Z total" vs "natural"). The non-viscose-related emissions in the Paris and Rouen areas explain almost half of this

discrepancy (24 ppt, "Z total" vs "ZviW + ZnviW + ZviB + ZnviB + ZviU"). The non-viscose-related emissions in "the rest of the world", i.e., the whole world excluding the Paris and Rouen areas and the Benelux explain a bit less than a quarter of the overestimation (12 ppt, "ZviW + ZnviW" vs "ZviW" vs "natural"). Of the remaining 12 ppt, 8 ppt are due to viscose industry emissions in the rest of the world and 1.5 ppt to viscose industry emissions in the Benelux alone. The unrealistic COS emissions

5 in the Paris and Rouen areas not only lead to too high median contributions but also to a large number of high concentration peaks, as shown by the upper elongation of the violin "Z total" (maximum actually > 1995 ppt). As expected, our home-made inventory is more compatible with the observations in GIF (Fig. 3). In this case, the background and the oceanic and biogenic land fluxes contribute for ≈40% to the median overestimation (≈4 ppt, Fig. 3: "GIF obs" vs "natural") of the observations, compared to 60% for the home-made anthropogenic emissions (≈7 ppt, Fig. 3: "HM total" vs "natural"). The distribution of

10 extreme events, i.e., with very high or very low COS concentrations obtained with our home-made inventory is closer to the observed one (Fig. 3, upper and lower elongations of "GIF obs" vs "Z total" vs "HM total").

Additional continuous observation sites would be needed in different places of Europe to clarify the relevancy of our inventory beyond the Paris area and vicinity.

3.3 Biogenic land fluxes

15 Disentangling the main contribution of mismatches between observations and simulations is very challenging with one site only. Differences at the synoptic scale, as represented in Fig. 1, can originate from erroneous background, transport discrepancies, or from incorrect fluxes. Still, as represented in the time series in Appendix A, fine scale temporal variability, corresponding to the diurnal cycle, is well reproduced during some periods of the year, especially in Spring. The diurnal cycle is dominated by local influences, with remote influence of the background and of distant fluxes transported to GIF filtered

20 out. We therefore focus here on 12-hour differences in measured or simulated COS concentrations, defined as either "daytime variation" between day D at 6 p.m. and day D at 6 a.m. or "nighttime variation" between day D+1 at 6 a.m. and day D at 6 p.m.. Thus, these differences are mostly influenced by a combination of small scale meteorological conditions (mostly the diurnal cycle of the planetary boundary layer) and of regional fluxes (within the transport footprint around the station).

The variations of the nighttime and daytime variations over the available 5.5 years of observation are represented in Fig. 4,

25 alongside COS fluxes from regional vegetation and soils. The observed seasonal cycle of night and day-time variations is similar for all years. The observed nighttime variations are slightly negative in winter (JFM; −7 ppt) then strongly negative in spring (AMJ; −10 ppt) with yearly peaks of ≈ −20 ppt; then, summer positive peaks of 10–15 ppt in July are followed by another negative low in fall (−8 ppt). The positive nighttime variations in summer are most probably due to emissions by the crops, such as rapeseed (Belviso et al., 2022a). Observed day-time variations are opposite with slightly different magnitudes.

30 In winter (JFM), the vegetation is mostly inactive in ORCHIDEE, and soils are at their lowest sink activity with the net soil uptake becoming larger than the vegetation uptake. Thus the contribution of the uptake by the vegetation and soils in our simulations for both time-resolutions (monthly or 3-hourly) is very small. Both the simulated variations are therefore close to zero (on average, −2 ppt for nighttime and +1 ppt for daytime), contrary to observed variations (−7 ppt for nighttime and
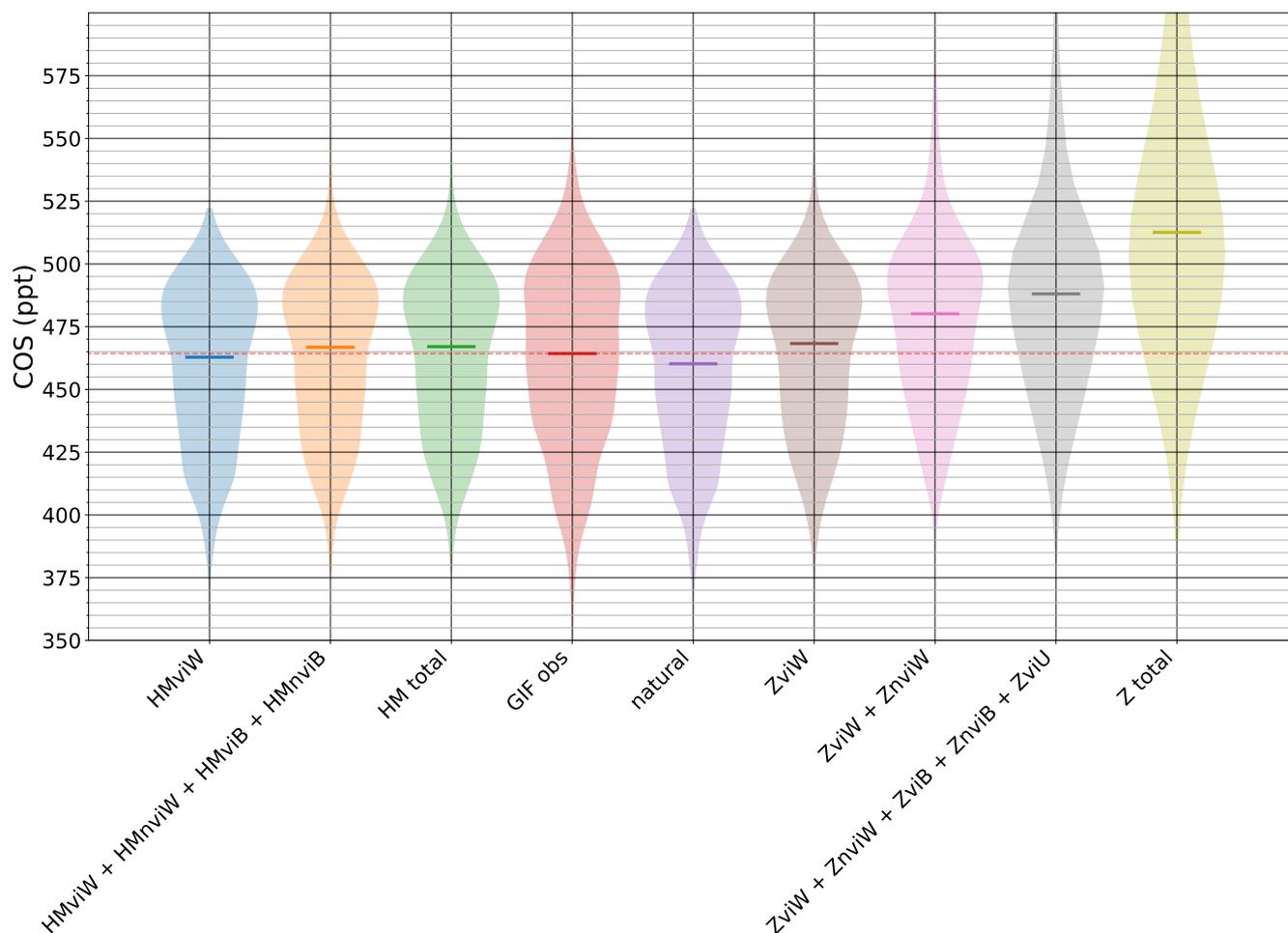
Figure 3. *Violin plots of COS mixing ratios at GIF (solid horizontal lines show the medians) for observations ("GIF obs") and various simulations taking into account different sets of contributions. See Tab. 1 for the available simulations per region and per sector; "natural" = background + o + bl; "Z total" = natural + ZviW + ZnviW + ZviB + ZnviB + ZviU + ZnviU; "HM total" = natural + HMviW + HMnviW + HMviB + HMnviB + HMviU + HMnviU.*
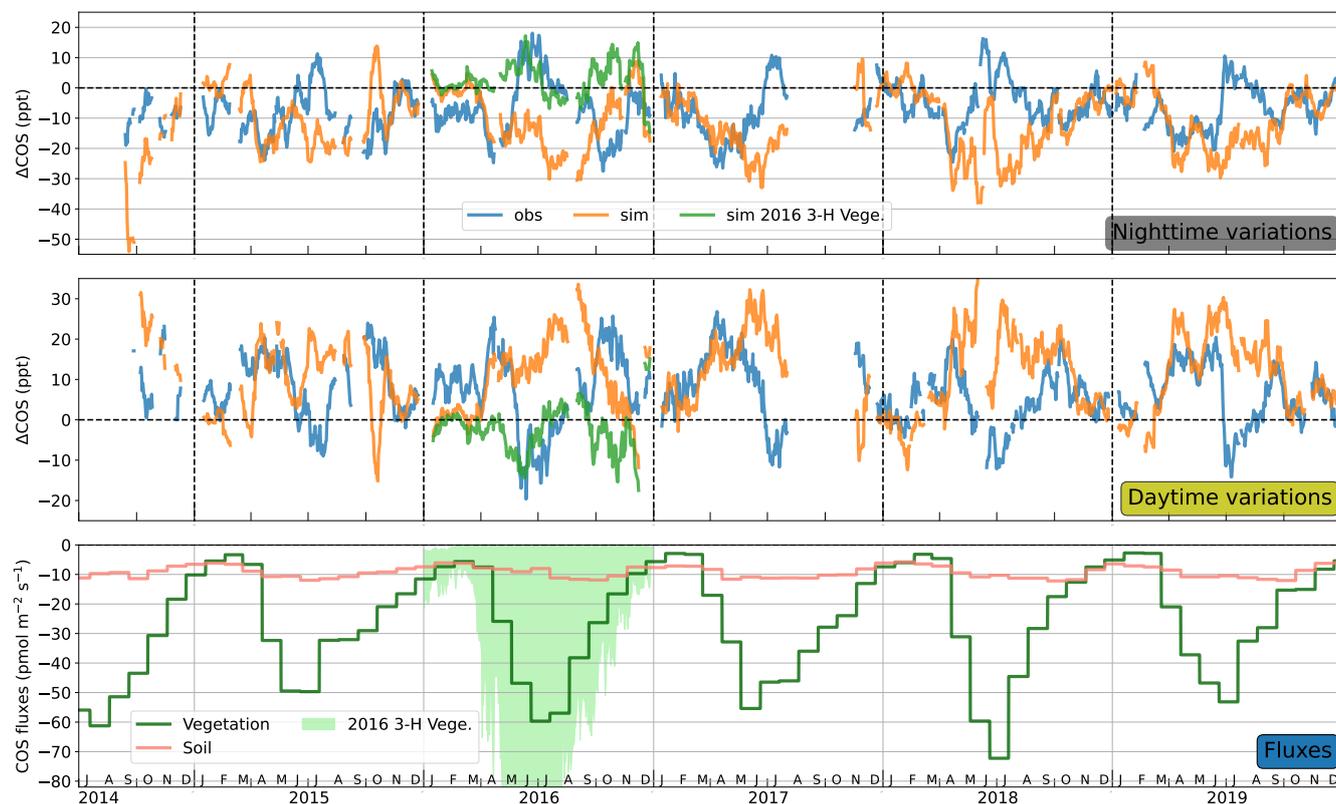
Figure 4. *15-day rolling mean of the nighttime (top) and daytime (middle) variations of the observed and simulated COS concentrations at GIF with matching COS total uptake by vegetation and soils in the domain of interest. Nighttime variation = $[COS]_{D@06:00} - [COS]_{D-1@18:00}$, daytime variation = $[COS]_{D@18:00} - [COS]_{D@06:00}$ (see text for more details); contributions taken into account in the simulations are the background + ocean + our home-made anthropogenic inventory + either biogenic land with a monthly time-resolution ("sim") or biogenic land with 2016 3-hourly time-resolution for vegetation ("sim 2016 3-H Vege."); fluxes are uptakes by the soil, the vegetation at a monthly ("Vegetation") or 3-hourly ("2016 3-H Vege.") resolution (see Sect. 2.2 for details).*

+7 ppt for daytime). This suggests under-estimated COS uptakes at night in winter in ORCHIDEE vegetation and/or soil datasets.

During spring (AMJ), vegetation COS uptake is activated in ORCHIDEE. When using constant monthly fluxes with no diurnal cycle, their contribution to the simulated nighttime uptake leads to lower concentrations at night compared to daytime, consistently with observations. In contrast, daytime concentrations are the result of compensating vegetation uptake and mixing in the boundary layer. However, the use of a more realistic 3-hourly vegetation uptake daily cycle results in simulated nighttime and daytime variation close to zero, not consistent with the observations. This discrepancy suggests a persistent nighttime uptake not adequately represented by ORCHIDEE's diurnal cycle, primarily based on photosynthesis uptake. Refining the model to improve the representation of nighttime processes may enhance its ability to reproduce observed dynamics. Summer

(JAS) shows opposite behavior compared to spring. Using a realistic diurnal cycle is key to reproducing the positive nighttime and negative daytime variations.

During fall (OND), the performance of our simulations exhibits variability across different years, regardless of the inclusion of a vegetation diurnal cycle. Notably, the simulations for the years 2016 and 2017 show significant discrepancies, whereas the
5   results for the remaining four years align well with observational data. This disparity underscores the challenges associated with accurately reproducing the timing of vegetation senescence, particularly given the influence of intricate synoptic meteorological conditions on both vegetation dynamics and the performance of the transport model. The complexity of these interactions poses a significant hurdle in achieving consistent simulation outcomes across all years.

4   Conclusions

10   The present study analyzes 5.5 years of quasi-continuous COS measurements from the site GIF in the Paris region. Through systematic comparison of measurements with simulations using backward trajectories computed with the Lagrangian model FLEXPART, we provide a quantitative assessment of natural and anthropogenic COS fluxes in Western Europe.

Regarding industrial-emitted COS, we highlight the unrealistic magnitude of anthropogenic fluxes as provided by Zumkehr's inventory (Zumkehr et al., 2018) in Europe. In particular, Zumkehr's inventory suggests very high emissions in the Paris area,
15   inconsistent with the absence of any coal power plant and major viscose industry in the region. We propose another inventory based on declared industrial emissions as well as coal power plants in Europe. The new inventory proves much more consistent with observations and includes only a limited number of emission hotspots in France. Still our inventory comes with several limitations. First, it takes into account the emissions as declared by the "industries"; this category includes only sources above a legally binding threshold. Therefore, we do not account for sources which are under the threshold and we assume them to
20   be small compared to the declared ones; but their overall magnitude remains actually unknown. Second, another limitation arise from the flat temporal variability applied to anthropogenic fluxes in our inventory (similarly to Zumkehr et al., 2018) due to the lack of information on industrial and power-generation activity in viscose factories and coal-power plants. This is expected to be a critical limiting factors as coal-power plant activity depends on energy demands, and viscose industry activity are often organized by batches with days of intense emissions followed by periods with limited emissions. Third, we apply
25   a single emission factor between CO_2 and COS emissions from coal-power plants, whereas this factor depends on the coal used in the combustion, as well as the overall properties and technologies used in the power-plant. Last, limitations are also due to the model-based approach of our study. The sources of COS or its precursors are stacks of factories or power plants, i.e., hot-spots: high sources localized in a very small area compared to the resolution of the chemistry-transport model used to simulate the concentrations. Therefore, the plumes emitted from these hot-spots are not always well represented by the model,
30   depending on the meteorological situation. For hot-spots close to the measurement site (e.g., from the Beauvais region 50 km North of GIF where viscose factories are active), the numerical diffusion of the plumes of COS represented in the model leads most of the time to underestimating simulated concentrations; in particular events, if the error on the wind direction is large enough, the plume may be unduly directed to the site in the model, which leads to overestimating the simulated concentrations.

Overcoming the above-mentioned limitations in assessing anthropogenic emissions would mostly need additional observation sites in the region (e.g., Zanchetta et al., 2023, in the Netherlands) to cross-validate our results.

Regarding soil and vegetation fluxes, we are able to suggest that the net ecosystem COS uptake simulated by ORCHIDEE is underestimated in winter at night, requiring improvements in the nighttime processes in land-process models. Even when using ORCHIDEE's vegetation and soil uptakes with a diurnal cycle at a 3-hourly resolution, the analysis of the simulated diurnal cycle of COS concentrations confirms that a night-time uptake is not adequately represented by ORCHIDEE, maybe due to the parameterization of the nighttime uptake by plants for COS.

Although it is based on only one site, the present study provides sufficient elements to identify discrepancies in COS emission data bases and land-process models in Western Europe, due to incorrect parameterizations of fluxes, or missing processes. Still, our single-site study is not sufficient to overcome those discrepancies to reach the level of precision needed to use COS observations as a proxy of plant uptake. A full network of observation sites, analog to the Integrated Carbon Observatory System (ICOS, Ramonet et al., 2011), would be a requirement to better quantify anthropogenic fluxes and thus to fully use COS for assessing CO_2 uptake by photosynthesis.

Code and data availability. GIF data is available from https://doi.org/10.14768/6800b065-dcec-4006-ada5-b5f62a4bb832. The CMIP6 version of the ORCHIDEE model including the vegetation and soil COS submodels is available upon request to the authors. Optimized COS concentration fields at the global scale by (Remaud et al., 2023) are available at https://zenodo.org/records/7632737 (OPT-LSCE).

Author contributions. AB designed and ran the simulations, including formatting of the home-made emission inventory and of observations; IP and AB analyzed the results, based on preliminary work by CH; CN and CH computed the FLEXPART simulations on which the analysis is based; MR provided the global COS inversions used to determine the background; SB provided the observations at GIF and the home-made French inventory of point sources; CA and FM provided ORCHIDEE fluxes; all co-authors contributed to writing the text.

Competing interests. The authors declare no competing interests relative to the present study.

Acknowledgements. This research has been supported by the 4C project of the European Commission's Horizon 2020 framework programme (Grant 821003). This study was partially funded by the CO2 Human Emissions (CHE) project, which received funding from the European Union's Horizon 2020 research and innovation programme under Grant 776186. Calculations were performed using the resources of LSCE, maintained by J. Bruna and the LSCE IT team.

References

Abadie, C., Maignan, F., Remaud, M., Ogée, J., Campbell, J. E., Whelan, M., Kitz, F., Spielmann, F., Wohlfahrt, G., Wehr, R., Sun, W., Raoult, N., Seibt, U., Hauglustaine, D., Lennartz, S., Belviso, S., Montagne, D., and Peylin, P.: Global modelling of soil carbonyl sulfide exchanges, Biogeosciences, 19, 2427, https://doi.org/10.5194/bg-19-2427-2022, 2022.

5 Attar, A.: Chemistry, thermodynamics and kinetics of reactions of sulphur in coal-gas reactions: A review, Fuel, 57, 201–212, https://doi.org/10.1016/0016-2361(78)90117-5, 1978.

Bandy, A. R., Maroulis, P. J., Shalaby, L., and Wilner, L. A.: Evidence for a short tropospheric residence time for carbon disulfide, Geophysical Research Letters, 8, 1180–1183, https://doi.org/10.1029/GL008i011p01180, _eprint: https://onlinelibrary.wiley.com/doi/pdf/10.1029/GL008i011p01180, 1981.

10 Barnes, I., Becker, K. H., and Patroescu, I.: The tropospheric oxidation of dimethyl sulfide: A new source of carbonyl sulfide, Geophysical Research Letters, 21, 2389–2392, https://doi.org/10.1029/94GL02499, _eprint: https://onlinelibrary.wiley.com/doi/pdf/10.1029/94GL02499, 1994.

Belviso, S., Reiter, I. M., Loubet, B., Gros, V., Lathière, J., Montagne, D., Delmotte, M., Ramonet, M., Kalogridis, C., Lebegue, B., Bonnaire, N., Kazan, V., Gauquelin, T., Fernandez, C., and Genty, B.: A top-down approach of surface carbonyl sulfide exchange by a Mediterranean
15 oak forest ecosystem in southern France, Atmospheric Chemistry and Physics, 16, 14 909–14 923, https://doi.org/10.5194/acp-16-14909-2016, publisher: Copernicus GmbH, 2016.

Belviso, S., Lebegue, B., Ramonet, M., Kazan, V., Pison, I., Berchet, A., Delmotte, M., Yver-Kwok, C., Montagne, D., and Ciais, P.: A top-down approach of sources and non-photosynthetic sinks of carbonyl sulfide from atmospheric measurements over multiple years in the Paris region (France), PLoS ONE, 15, e0228 419, https://doi.org/10.1371/journal.pone.0228419, 2020.

20 Belviso, S., Abadie, C., Montagne, D., Hadjar, D., Tropée, D., Vialettes, L., Kazan, V., Delmotte, M., Maignan, F., Remaud, M., Ramonet, M., Lopez, M., Yver-Kwok, C., and Ciais, P.: Carbonyl sulfide (COS) emissions in two agroecosystems in central France, PLoS ONE, 17, e0278 584, https://doi.org/10.1371/journal.pone.0278584, 2022a.

Belviso, S., Remaud, M., Abadie, C., Maignan, F., Ramonet, M., and Peylin, P.: Ongoing Decline in the Atmospheric COS Seasonal Cycle Amplitude over Western Europe: Implications for Surface Fluxes, Atmosphere, 13, 812, https://doi.org/10.3390/atmos13050812, 2022b.

25 Belviso, S., Pison, I., Petit, J.-E., Berchet, A., Remaud, M., Simon, L., Ramonet, M., Delmotte, M., Kazan, V., Yver-Kwok, C., and Lopez, M.: The Z-2018 emissions inventory of COS in Europe: A semiquantitative multi-data-streams evaluation, Atmospheric Environment, 300, 119 689, https://doi.org/10.1016/j.atmosenv.2023.119689, 2023.

Berchet, A., Sollum, E., Pison, I., Thompson, R. L., Thanwerdas, J., Fortems-Cheiney, A., Peet, J. C. A. v., Potier, E., Chevallier, F., Broquet, G., and Adrien, B.: The Community Inversion Framework: codes and documentation, https://doi.org/10.5281/zenodo.5045730, 2021.

30 Berchet, A., Pison, I., and Narbaud, C.: FLEXPART-GUI-toolbox, https://doi.org/10.5281/zenodo.7766372, 2023.

Berry, J., Wolf, A., Campbell, J. E., Baker, I., Blake, N., Blake, D., Denning, A. S., Kawa, S. R., Montzka, S. A., Seibt, U., Stimler, K., Yakir, D., and Zhu, Z.: A coupled model of the global cycles of carbonyl sulfide and CO2: A possible new window on the carbon cycle, Journal of Geophysical Research: Biogeosciences, 118, 842–852, https://doi.org/10.1002/jgrg.20068, _eprint: https://onlinelibrary.wiley.com/doi/pdf/10.1002/jgrg.20068, 2013.

35 Bloem, E., Haneklaus, S., Kesselmeier, J., and Schnug, E.: Sulfur Fertilization and Fungal Infections Affect the Exchange of H2S and COS from Agricultural Crops, Journal of Agricultural and Food Chemistry, 60, 7588–7596, https://doi.org/10.1021/jf301912h, 2012.

Brownlee, B. G., Kenefick, S. L., Maclnnis, G. A., and Hrudey, S. E.: Characterization of odorous compounds from bleached kraft pulp mill effluent, Water Science and Technology, 31, 35–40, https://doi.org/10.1016/0273-1223(95)00453-T, 1995.

Chen, J.: Chapter 4 - Synthetic Textile Fibers: Regenerated Cellulose Fibers, in: Textiles and Fashion, edited by Sinclair, R., Woodhead Publishing Series in Textiles, pp. 79–95, Woodhead Publishing, ISBN 978-1-84569-931-4, https://doi.org/10.1016/B978-1-84569-931-4.00004-0, 2015.

Cheremisinoff, N. P. and Rosenfeld, P. E.: Chapter 6 - Sources of air emissions from pulp and paper mills, in: Handbook of Pollution Prevention and Cleaner Production, edited by Cheremisinoff, N. P. and Rosenfeld, P. E., pp. 179–259, William Andrew Publishing, Oxford, ISBN 978-0-08-096446-1, https://doi.org/https://doi.org/10.1016/B978-0-08-096446-1.10006-1, 2010.

Chin, M. and Davis, D. D.: Global sources and sinks of OCS and CS2 and their distributions, Global Biogeochemical Cycles, 7, 321–337, https://doi.org/10.1029/93GB00568, _eprint: https://onlinelibrary.wiley.com/doi/pdf/10.1029/93GB00568, 1993.

Commane, R., Meredith, L. K., Baker, I. T., Berry, J. A., Munger, J. W., Montzka, S. A., Templer, P. H., Juice, S. M., Zahniser, M. S., and Wofsy, S. C.: Seasonal fluxes of carbonyl sulfide in a midlatitude forest, Proceedings of the National Academy of Sciences, 112, 14 162–14 167, https://doi.org/10.1073/pnas.1504131112, publisher: Proceedings of the National Academy of Sciences, 2015.

DiMario, R. J., Quebedeaux, J. C., Longstreth, D. J., Dassanayake, M., Hartman, M. M., and Moroney, J. V.: The Cytoplasmic Carbonic Anhydrases βCA2 and βCA4 Are Required for Optimal Plant Growth at Low CO2, Plant Physiol, 171, 280–293, https://doi.org/10.1104/pp.15.01990, 2016.

Du, Q., Mu, Y., Zhang, C., Liu, J., Zhang, Y., and Liu, C.: Photochemical production of carbonyl sulfide, carbon disulfide and dimethyl sulfide in a lake water, Journal of Environmental Sciences, 51, 146–156, https://doi.org/10.1016/j.jes.2016.08.006, 2017.

Harnisch, J., Borchers, R., and Fabian, P.: COS, CS2 and SO2 in aluminium smelter exhaust, Environ. Sci. & Pollut. Res., 2, 229–232, https://doi.org/10.1007/BF02986771, 1995.

Hersbach, H., Bell, B., Berrisford, P., Hirahara, S., Horányi, A., Muñoz-Sabater, J., Nicolas, J., Peubey, C., Radu, R., Schepers, D., Simmons, A., Soci, C., Abdalla, S., Abellan, X., Balsamo, G., Bechtold, P., Biavati, G., Bidlot, J., Bonavita, M., De Chiara, G., Dahlgren, P., Dee, D., Diamantakis, M., Dragani, R., Flemming, J., Forbes, R., Fuentes, M., Geer, A., Haimberger, L., Healy, S., Hogan, R. J., Hólm, E., Janisková, M., Keeley, S., Laloyaux, P., Lopez, P., Lupu, C., Radnoti, G., de Rosnay, P., Rozum, I., Vamborg, F., Villaume, S., and Thépaut, J.-N.: The ERA5 global reanalysis, Quarterly Journal of the Royal Meteorological Society, 146, 1999–2049, https://doi.org/10.1002/qj.3803, _eprint: https://onlinelibrary.wiley.com/doi/pdf/10.1002/qj.3803, 2020.

Kamezaki, K., Danielache, S. O., Ishidoya, S., Maeda, T., and Murayama, S.: Development of compact continuous measurement system for atmospheric carbonyl sulfide concentration, Atmospheric Measurement Techniques Discussions, pp. 1–22, https://doi.org/10.5194/amt-2023-209, publisher: Copernicus GmbH, 2023.

Khalil, M. A. K. and Rasmussen, R. A.: Global sources, lifetimes and mass balances of carbonyl sulfide (OCS) and carbon disulfide (CS2) in the earth's atmosphere, Atmospheric Environment (1967), 18, 1805–1813, https://doi.org/10.1016/0004-6981(84)90356-1, 1984.

Kitz, F., Gerdel, K., Hammerle, A., Laterza, T., Spielmann, F. M., and Wohlfahrt, G.: In situ soil COS exchange of a temperate mountain grassland under simulated drought, Oecologia, 183, 851–860, https://doi.org/10.1007/s00442-016-3805-0, 2017.

Kitz, F., Spielmann, F. M., Hammerle, A., Kolle, O., Migliavacca, M., Moreno, G., Ibrom, A., Krasnov, D., Noe, S. M., and Wohlfahrt, G.: Soil COS Exchange: A Comparison of Three European Ecosystems, Global Biogeochemical Cycles, 34, e2019GB006 202, https://doi.org/10.1029/2019GB006202, _eprint: https://onlinelibrary.wiley.com/doi/pdf/10.1029/2019GB006202, 2020.

Kooijmans, L. M. J., Uitslag, N. A. M., Zahniser, M. S., Nelson, D. D., Montzka, S. A., and Chen, H.: Continuous and high-precision atmospheric concentration measurements of COS, CO_2, CO and H_2O using a quantum cascade laser spectrometer (QCLS), Atmospheric Measurement Techniques, 9, 5293–5314, https://doi.org/10.5194/amt-9-5293-2016, publisher: Copernicus GmbH, 2016.

Kooijmans, L. M. J., Cho, A., Ma, J., Kaushik, A., Haynes, K. D., Baker, I., Luijkx, I. T., Groenink, M., Peters, W., Miller, J. B., Berry, J. A.,
5   Ogée, J., Meredith, L. K., Sun, W., Kohonen, K.-M., Vesala, T., Mammarella, I., Chen, H., Spielmann, F. M., Wohlfahrt, G., Berkelhammer, M., Whelan, M. E., Maseyk, K., Seibt, U., Commane, R., Wehr, R., and Krol, M.: Evaluation of carbonyl sulfide biosphere exchange in the Simple Biosphere Model (SiB4), Biogeosciences, 18, 6547–6565, https://doi.org/10.5194/bg-18-6547-2021, 2021.

Krinner, G., Viovy, N., de Noblet-Ducoudré, N., Ogée, J., Polcher, J., Friedlingstein, P., Ciais, P., Sitch, S., and Prentice, I. C.: A dynamic global vegetation model for studies of the coupled atmosphere-biosphere system, Global Biogeochemical Cycles, 19,
10   https://doi.org/https://doi.org/10.1029/2003GB002199, 2005.

Lennartz, S. T., Marandino, C. A., von Hobe, M., Cortes, P., Quack, B., Simo, R., Booge, D., Pozzer, A., Steinhoff, T., Arevalo-Martinez, D. L., Kloss, C., Bracher, A., Röttgers, R., Atlas, E., and Krüger, K.: Direct oceanic emissions unlikely to account for the missing source of atmospheric carbonyl sulfide, Atmospheric Chemistry and Physics, 17, 385–402, https://doi.org/10.5194/acp-17-385-2017, publisher: Copernicus GmbH, 2017.

15 Lennartz, S. T., Gauss, M., von Hobe, M., and Marandino, C. A.: Monthly resolved modelled oceanic emissions of carbonyl sulphide and carbon disulphide for the period 2000–2019, Earth System Science Data, 13, 2095–2110, https://doi.org/10.5194/essd-13-2095-2021, publisher: Copernicus GmbH, 2021.

Ma, J., Remaud, M., Peylin, P., Patra, P., Niwa, Y., Rodenbeck, C., Cartwright, M., Harrison, J. J., Chipperfield, M. P., Pope, R. J., Wilson, C., Belviso, S., Montzka, S. A., Vimont, I., Moore, F., Atlas, E. L., Schwartz, E., and Krol, M. C.: Intercomparison of At-
20   mospheric Carbonyl Sulfide (TransCom-COS): 2. Evaluation of Optimized Fluxes Using Ground-Based and Aircraft Observations, Journal of Geophysical Research: Atmospheres, 128, e2023JD039 198, https://doi.org/https://doi.org/10.1029/2023JD039198, _eprint: https://agupubs.onlinelibrary.wiley.com/doi/pdf/10.1029/2023JD039198, 2023.

Maignan, F., Abadie, C., Remaud, M., Kooijmans, L. M. J., Kohonen, K.-M., Commane, R., Wehr, R., Campbell, J. E., Belviso, S., Montzka, S. A., Raoult, N., Seibt, U., Shiga, Y. P., Vuichard, N., Whelan, M. E., and Peylin, P.: Carbonyl sulfide: comparing a mechanistic rep-
25   resentation of the vegetation uptake in a land surface model and the leaf relative uptake approach, Biogeosciences, 18, 2917–2955, https://doi.org/10.5194/bg-18-2917-2021, publisher: Copernicus GmbH, 2021.

Masaki, Y., Iizuka, R., Kato, H., Kojima, Y., Ogawa, T., Yoshida, M., Matsushita, Y., and Katayama, Y.: Fungal Carbonyl Sulfide Hydrolase of Trichoderma harzianum Strain THIF08 and Its Relationship with Clade D β-Carbonic Anhydrases, Microbes Environ, 36, ME20 058, https://doi.org/10.1264/jsme2.ME20058, 2021.

30 Maseyk, K., Berry, J. A., Billesbach, D., and Seibt, U.: Sources and sinks of carbonyl sulfide in an agricultural field in the Southern Great Plains, P. Natl. Acad. Sci. USA, 111, https://doi.org/10.1073/pnas.1319132111, 2014.

Mihalopoulos, N., Nguyen, B. C., Putaud, J. P., and Belviso, S.: The oceanic source of carbonyl sulfide (COS), Atmospheric Environment. Part A. General Topics, 26, 1383–1394, https://doi.org/10.1016/0960-1686(92)90123-3, 1992.

Montzka, S. A., Calvert, P., Hall, B. D., Elkins, J. W., Conway, T. J., Tans, P. P., and Sweeney, C.: On the global distribution, seasonality,
35   and budget of atmospheric carbonyl sulfide (COS) and some similarities to CO2, Journal of Geophysical Research: Atmospheres, 112, https://doi.org/10.1029/2006JD007665, _eprint: https://onlinelibrary.wiley.com/doi/pdf/10.1029/2006JD007665, 2007.

Ogée, J., Sauze, J., Kesselmeier, J., Genty, B., Van Diest, H., Launois, T., and Wingate, L.: A new mechanistic framework to predict OCS fluxes from soils, Biogeosciences, 13, 2221–2240, https://doi.org/10.5194/bg-13-2221-2016, publisher: Copernicus GmbH, 2016.

Pisso, I., Sollum, E., Grythe, H., Kristiansen, N. I., Cassiani, M., Eckhardt, S., Arnold, D., Morton, D., Thompson, R. L., Groot Zwaaftink, C. D., Evangeliou, N., Sodemann, H., Haimberger, L., Henne, S., Brunner, D., Burkhart, J. F., Fouilloux, A., Brioude, J., Philipp, A., Seibert, P., and Stohl, A.: The Lagrangian particle dispersion model FLEXPART version 10.4, Geoscientific Model Development, 12, 4955–4997, https://doi.org/https://doi.org/10.5194/gmd-12-4955-2019, publisher: Copernicus GmbH, 2019.

5   Protoschill-Krebs, G., Wilhelm, C., and Kesselmeier, J.: Consumption of carbonyl sulphide (COS) by higher plant carbonic anhydrase (CA), Atmospheric Environment, 30, 3151–3156, https://api.semanticscholar.org/CorpusID:84856936, 1996.

Ramonet, M., Ciais, P., Rivier, L., Laurila, T., Vermeulen, A., Geever, M., Jordan, A., Levin, I., Laurent, O., Delmotte, M., Wastine, B., Hazan, L., Schmidt, M., Tarniewicz, J., Vuillemin, C., Pison, I., Spain, G., and Paris, J.-D.: The ICOS Atmospheric Thematic Center (ATC), GAW Report No. 206, 16th WMO/IAEA Meeting on Carbon Dioxide, Other Greenhouse Gases and Related Tracers Measurement Techniques
10 (GGMT-2011), 2011.

Remaud, M., Chevallier, F., Maignan, F., Belviso, S., Berchet, A., Parouffe, A., Abadie, C., Bacour, C., Lennartz, S., and Peylin, P.: Plant gross primary production, plant respiration and carbonyl sulfide emissions over the globe inferred by atmospheric inverse modelling, Atmospheric Chemistry and Physics, 22, 2525–2552, https://doi.org/10.5194/acp-22-2525-2022, publisher: Copernicus GmbH, 2022.

Remaud, M., Ma, J., Krol, M., Abadie, C., Cartwright, M. P., Patra, P., Niwa, Y., Rodenbeck, C., Belviso, S., Kooijmans, L., Lennartz,
15 S., Maignan, F., Chevallier, F., Chipperfield, M. P., Pope, R. J., Harrison, J. J., Vimont, I., Wilson, C., and Peylin, P.: Intercomparison of Atmospheric Carbonyl Sulfide (TransCom-COS; Part One): Evaluating the Impact of Transport and Emissions on Tropospheric Variability Using Ground-Based and Aircraft Data, Journal of Geophysical Research: Atmospheres, 128, e2022JD037 817, https://doi.org/https://doi.org/10.1029/2022JD037817, 2023.

Sandoval-Soto, L., Stanimirov, M., Hobe, M. v., Schmitt, V., Valdes, J., Wild, A., and Kesselmeier, J.: Global uptake of carbonyl sulfide (COS)
20 by terrestrial vegetation: Estimates corrected by deposition velocities normalized to the uptake of carbon dioxide (CO_2), Biogeosciences, 2, 125–132, https://api.semanticscholar.org/CorpusID:16099750, 2005.

Seibert, P. and Frank, A.: Source-receptor matrix calculation with a Lagrangian particle dispersion model in backward mode, Atmospheric Chemistry and Physics, 4, 51–63, https://doi.org/10.5194/acp-4-51-2004, 2004.

Stickel, R. E., Chin, M., Daykin, E. P., Hynes, A. J., Wine, P. H., and Wallington, T. J.: Mechanistic studies of the hydroxyl-initiated oxidation
25 of carbon disulfide in the presence of oxygen, The Journal of Physical Chemistry, 97, 13 653–13 661, https://doi.org/10.1021/j100153a038, publisher: American Chemical Society, 1993.

Stinecipher, J., Cameron-Smith, P., Blake, N., Kuai, L., Lejeune, B., Mahieu, E., Simpson, I., and Campbell, J.: Biomass Burning Unlikely to Account for Missing Source of Carbonyl Sulfide, Geophysical Research Letters, 46, 14 912–14 920, https://doi.org/10.1029/2019GL085567, _eprint: https://onlinelibrary.wiley.com/doi/pdf/10.1029/2019GL085567, 2019.

30 Stohl, A., Forster, C., Frank, A., Seibert, P., Wotawa, G., et al.: Technical note: The Lagrangian particle dispersion model FLEXPART version 6.2, Atmos. Chem. Phys., 5, 2461–2474, http://hal-insu.archives-ouvertes.fr/hal-00301615/, 2005.

Thompson, R. L. and Stohl, A.: FLEXINVERT: an atmospheric Bayesian inversion framework for determining surface fluxes of trace species using an optimized grid, Geoscientific Model Development, 7, 2223–2242, https://doi.org/10.5194/gmd-7-2223-2014, publisher: Copernicus GmbH, 2014.

35 Tipka, A., Haimberger, L., and Seibert, P.: Flex_extract v7.1.2 – a software package to retrieve and prepare ECMWF data for use in FLEXPART, Geoscientific Model Development, 13, 5277–5310, https://doi.org/10.5194/gmd-13-5277-2020, publisher: Copernicus GmbH, 2020.

Water, U. S. E. P. A. O. o.: Preliminary Study of Carbon Disulfide Discharges from Cellulose Products Manufacturers, Tech. Rep. 821-R-11-009, United States Environmental Protection Agency, https://www.epa.gov/sites/production/files/2015-10/documents/cellulose-products_prelimstudy_2011.pdf, 2011.

Whelan, M., Lennartz, S., Gimeno, T., Wehr, R., Wohlfahrt, G., Wang, Y., Kooijmans, L., Hilton, T., Belviso, S., Peylin, P., Commane, R.,
5   Sun, W., Chen, H., Kuai, L., Mammarella, I., Maseyk, K., Berkelhammer, M., Li, K.-F., Yakir, D., Zumkehr, A., Katayama, Y., Ogée, J., Spielmann, F., Kitz, F., Rastogi, B., Kesselmeier, J., Marshall, J., Erkkilä, K.-M., Wingate, L., Meredith, L., He, W., Bunk, R., Launois, T., Vesala, T., Schmidt, J., Fichot, C. G., Seibt, U., Saleska, S., Saltzman, E., Montzka, S., Berry, J., and Campbell, J. E.: Reviews and syntheses: Carbonyl sulfide as a multi-scale tracer for carbon and water cycles, Biogeosciences, 15, 3625, https://doi.org/10.5194/bg-15-3625-2018, 2018.

10   Whelan, M. E. and Rhew, R. C.: Carbonyl sulfide produced by abiotic thermal and photodegradation of soil organic matter from wheat field substrate, Journal of Geophysical Research: Biogeosciences, 120, 54–62, https://doi.org/10.1002/2014JG002661, _eprint: https://onlinelibrary.wiley.com/doi/pdf/10.1002/2014JG002661, 2015.

Whelan, M. E., Hilton, T. W., Berry, J. A., Berkelhammer, M., Desai, A. R., and Campbell, J. E.: Carbonyl sulfide exchange in soils for better estimates of ecosystem carbon uptake, Atmospheric Chemistry and Physics, 16, 3711–3726, https://doi.org/10.5194/acp-16-3711-2016,
15   publisher: Copernicus GmbH, 2016.

Zanchetta, A., Kooijmans, L. M. J., van Heuven, S., Scifo, A., Scheeren, H. A., Mammarella, I., Karstens, U., Ma, J., Krol, M., and Chen, H.: Sources and sinks of carbonyl sulfide inferred from tower and mobile atmospheric observations in the Netherlands, Biogeosciences, 20, 3539–3553, https://doi.org/10.5194/bg-20-3539-2023, publisher: Copernicus GmbH, 2023.

Zumkehr, A., Hilton, T. W., Whelan, M., Smith, S., Kuai, L., Worden, J., and Campbell, J. E.: Global gridded anthropogenic emissions
20   inventory of carbonyl sulfide, Atmospheric Environment, 183, 11–19, https://doi.org/10.1016/j.atmosenv.2018.03.063, 2018.

Appendix A: Time series of observations and simulations
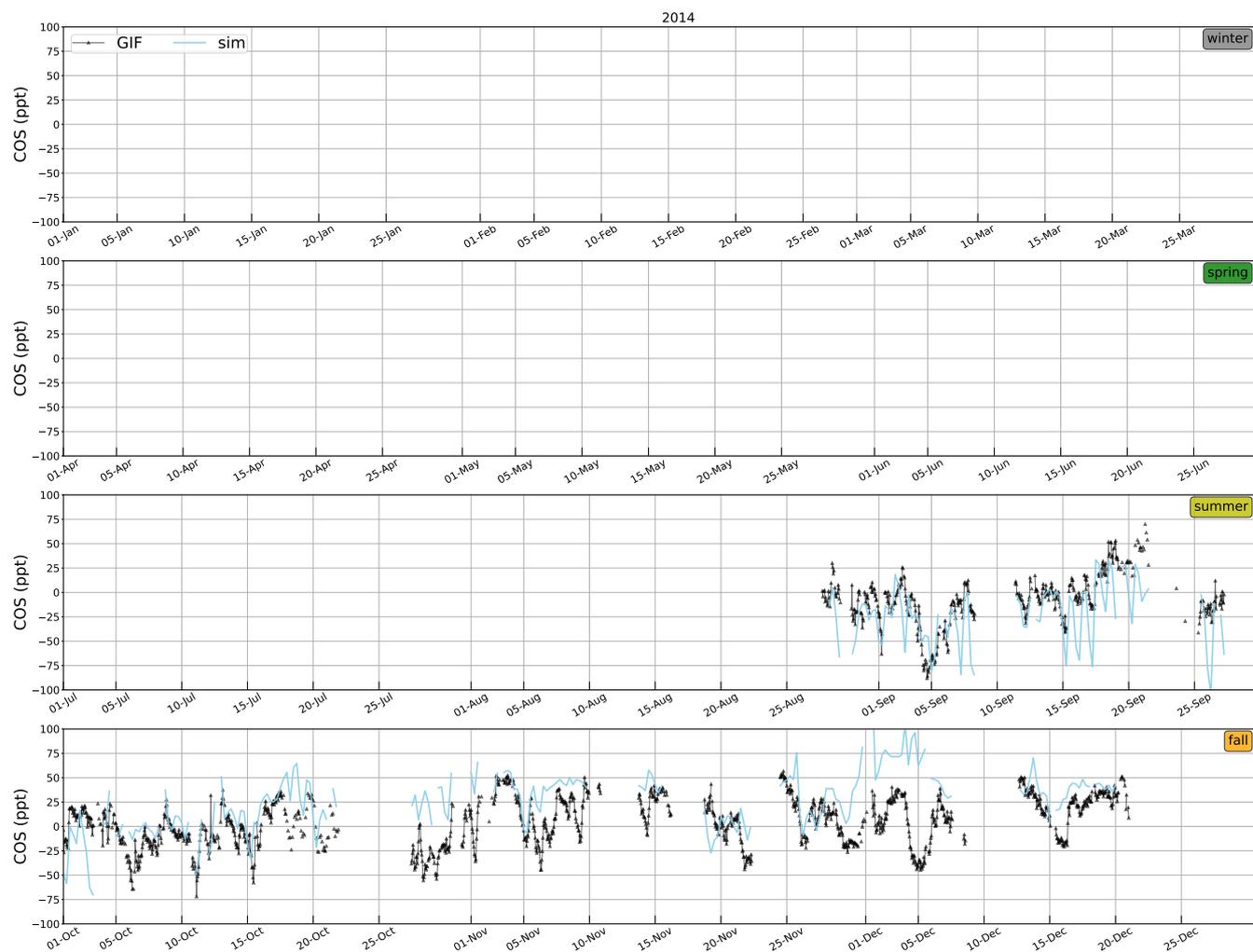
Figure A1. *Smoothed time series of observed and simulated atmospheric mixing ratios of COS at GIF in 2014. Observations are hourly averages; contributions taken into account in the simulations are the background + ocean + our home-made anthropogenic inventory + biogenic land with a monthly time-resolution for vegetation and soils (see Sect. 2.2 for details); smoothed by substracting the rolling 20-day mean of the observations to the observed and simulated time series. Note that the time series begins end of August 2014.*
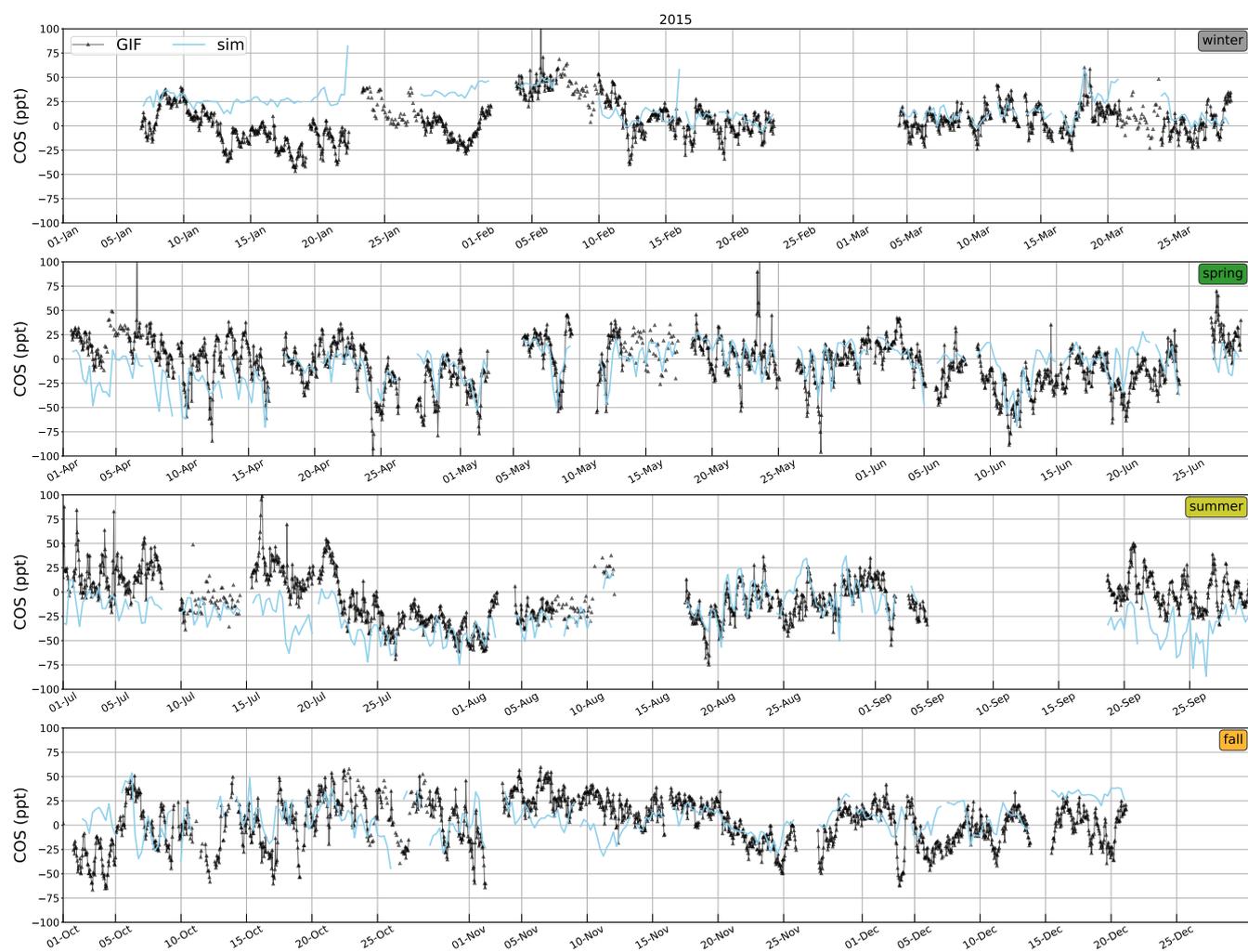
Figure A2. *Same as Fig. A1 for year 2015.*
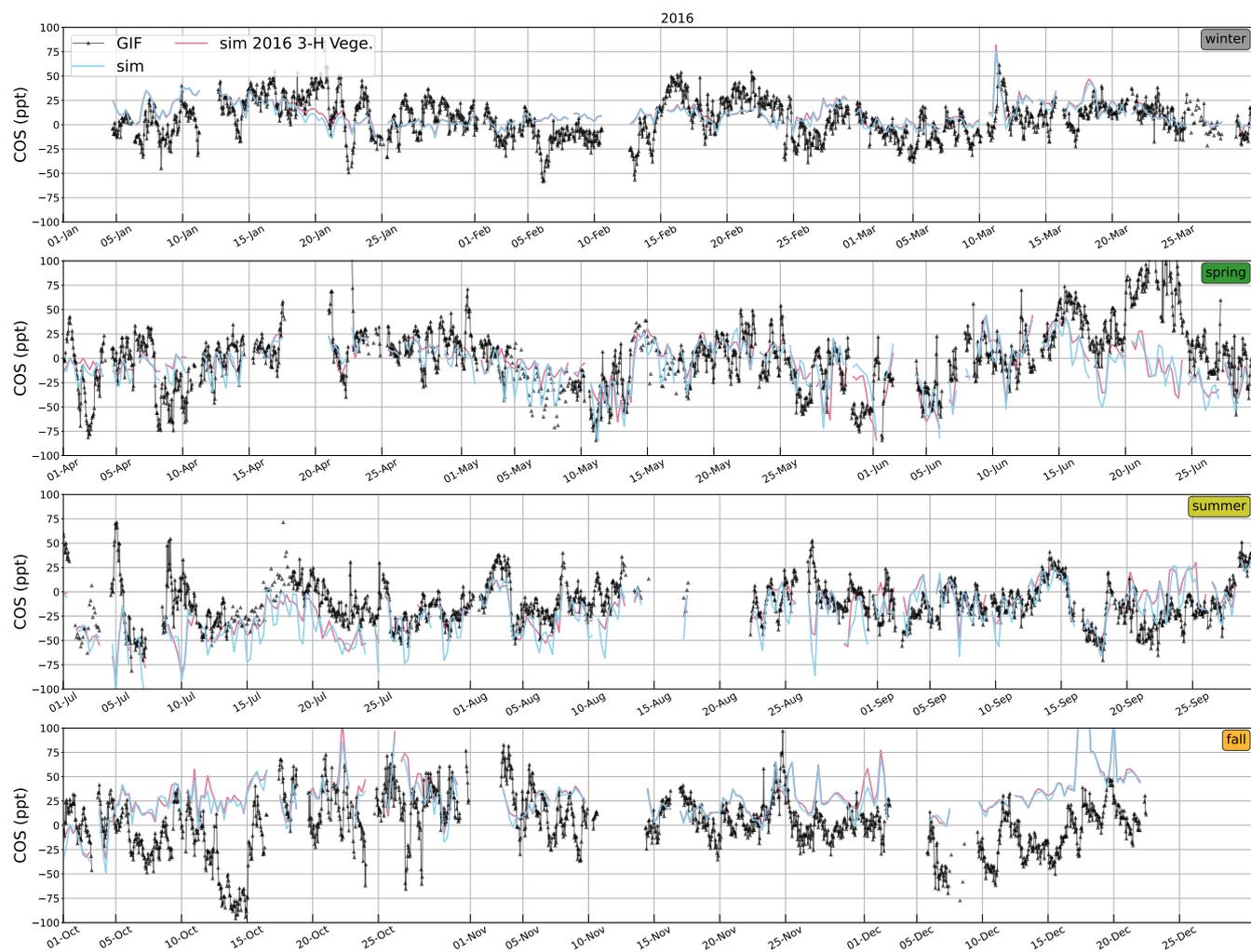
Figure A3. *Same as Fig. A1 for year 2016, with simulated contribution from the vegetation uptake with 3-hourly time-resolution (see Sect. 2.2 for details).*
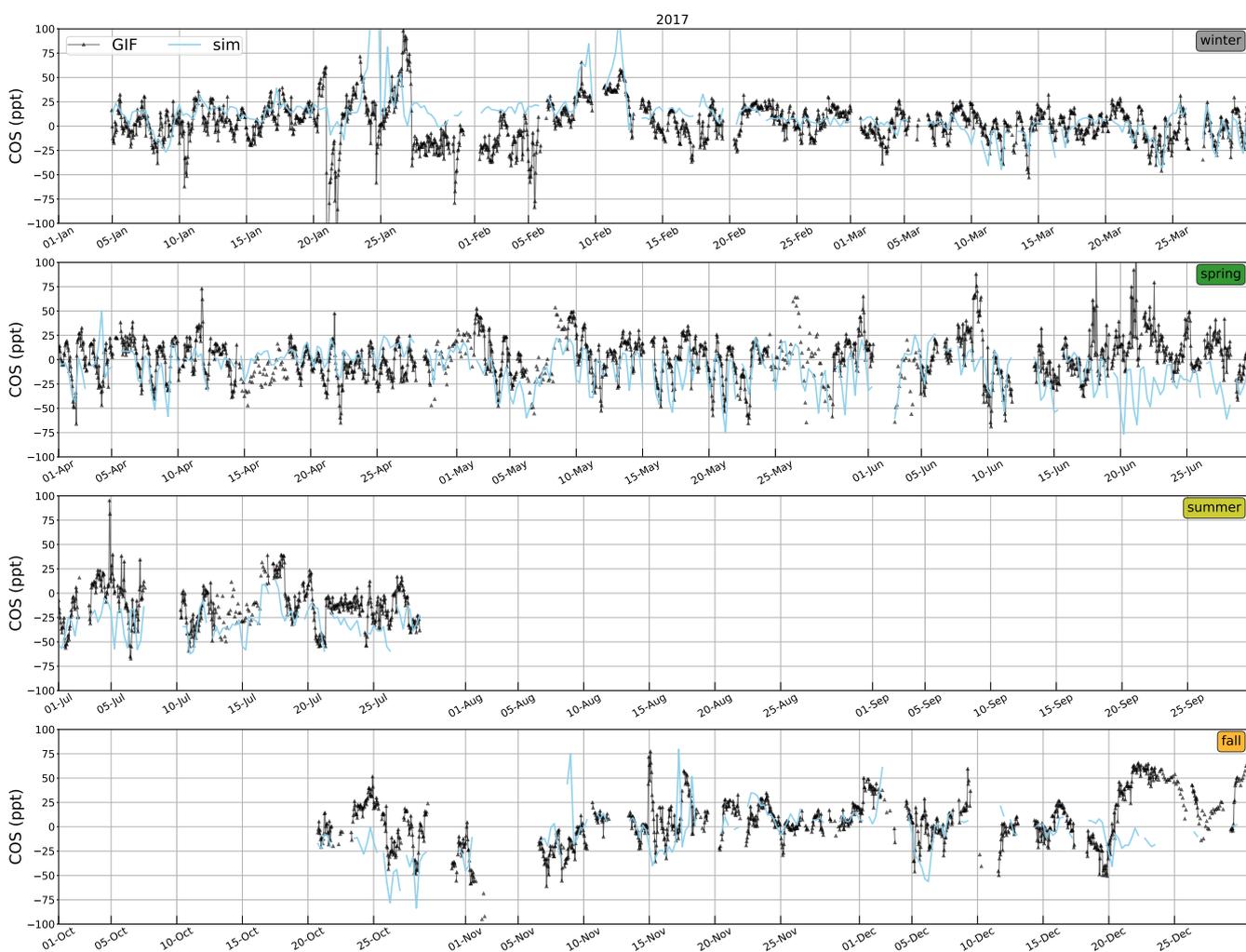
Figure A4. *Same as Fig. A1 for year 2017.*
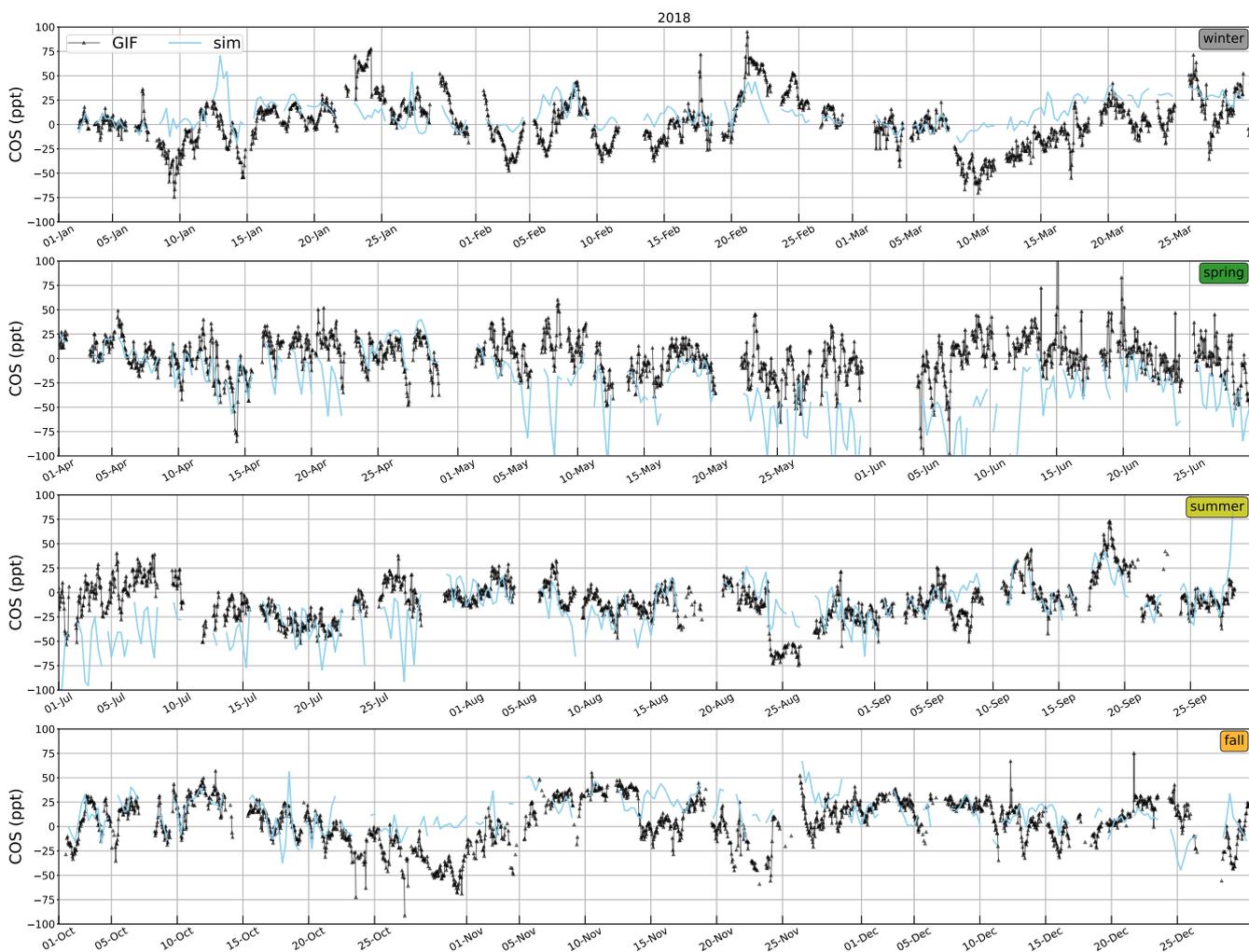
Figure A5. *Same as Fig. A1 for year 2018.*
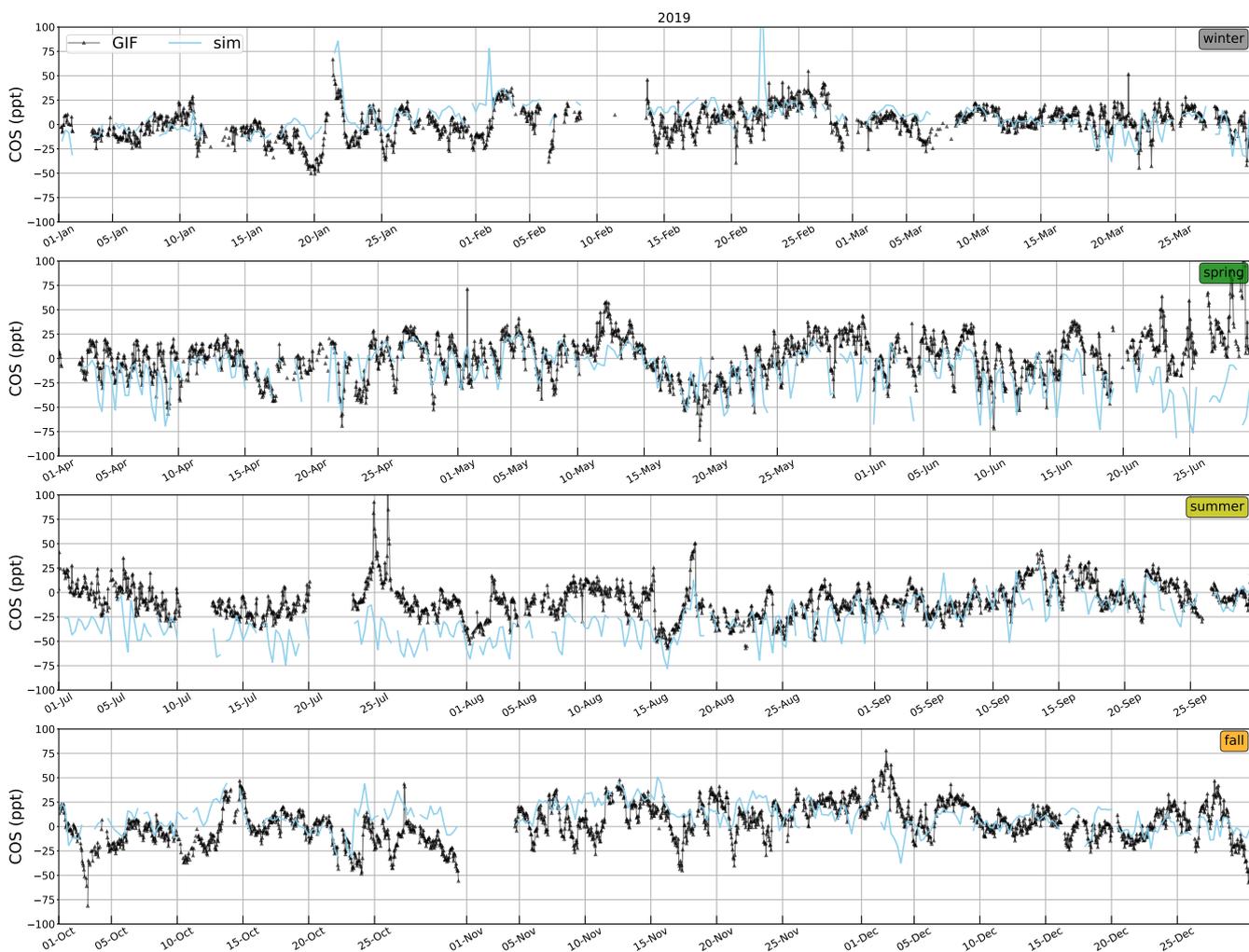
Figure A6. *Same as Fig. A1 for year 2019.*